(d) Answer (a), (b) and (c) for an Al–2 wt% Cu alloy solidified under the same conditions.

4.16 (a) Using Equation 4.33 and the data in problem 4.15 plot the variation of copper concentration along a unidirectionally solidified bar of an Al–2 wt% Cu alloy assuming no diffusion in the solid and perfect mixing in the liquid.
(b) What fraction of the bar will solidify to a eutectic structure?
(c) How much eutectic would form in an Al–0.5 wt% Cu alloy solidified under the same conditions?

4.17 Explain the experimental observation that in the presence of a convection current cells grow upstream.

4.18 Sketch a possible solidification-front structure for the solidification of an Fe–0.25 wt% C alloy in a shallow temperature gradient. Consider the temperature range 1440–1540 °C. Assume very rapid diffusion of carbon in δ–Fe.

4.19 Show that the condition $\lambda = 2\lambda^*$ gives (i) the maximum eutectic growth rate for a given undercooling, and (ii) a minimum undercooling for a given growth rate (Equation 4.43).

4.20 Calculate the depression of the eutectic temperature for a lamellar eutectic with $\lambda = 0.2$ μm and $\lambda = 1.0$ μm, if $\gamma_{\alpha\beta} = 400$ mJ m^{-2}, $\Delta H/V_m = 800 \times 10^6$ J m^{-3}, $T_E = 1000$ K.

4.21 If it is assumed that the choice of a rod or lamellar eutectic is governed by the minimization of the total α/β interfacial energy it can be shown that for a given λ there is a critical volume fraction of the β phase (f_c) below which β should be rod like, and above which it should be lamellar. Assuming the rods are hexagonally arranged and that $\gamma_{\alpha\beta}$ is isotropic, calculate the value of f_c.

4.22 Compare the processes of ingot casting and weld solidification, and show they are in many ways quite different solidification processes. How would you compare continuous casting in this respect?

4.23 What is the influence of welding speed on the solidification structure of welds? How is welding speed likely to affect segregation problems?

5
Diffusional Transformations in Solids

The majority of phase transformations that occur in the solid state take place by thermally activated atomic movements. The transformations that will be dealt with in this chapter are those that are induced by a change of temperature of an alloy that has a fixed bulk composition. Usually we will be concerned with the transformations caused by a temperature change from a single-phase region of a (binary) phase diagram to a region where one or more other phases are stable. The different types of phase transformations that are possible can be roughly divided into the following groups: (a) precipitation reactions, (b) eutectoid transformations, (c) ordering reactions, (d) massive transformations, and (e) polymorphic changes. Figure 5.1 shows several different types of binary phase diagrams that are representative of these transformations.

Precipitation transformations can be expressed in reaction terms as follows

$$\alpha' \rightarrow \alpha + \beta \tag{5.1}$$

where α′ is a metastable *supersaturated solid solution*, β is a stable or metastable precipitate, and α is a more stable solid solution with the same crystal structure as α′, but with a composition closer to equilibrium, see Fig. 5.1a.

Eutectoid transformations involve the replacement of a metastable phase (γ) by a more stable mixture of two other phases (α + β) and can be expressed as

$$\gamma \rightarrow \alpha + \beta \tag{5.2}$$

This reaction is characteristic of phase diagrams such as that shown in Fig. 5.1b.

Both precipitation and eutectoid transformations involve the formation of phases with a different composition to the matrix and therefore long-range diffusion is required. The remaining reaction types can, however, proceed without any composition change or long-range diffusion. Figure 5.1c shows phase diagrams where *ordering reactions* can occur. In this case the reaction can be simply written

$$\alpha(\text{disordered}) \rightarrow \alpha'(\text{ordered}) \tag{5.3}$$

In a *massive* transformation the original phase decomposes into one or more new phases which have the same composition as the parent phase, but different crystal structures. Figure 5.1d illustrates two simple examples of the type

$$\beta \rightarrow \alpha \tag{5.4}$$

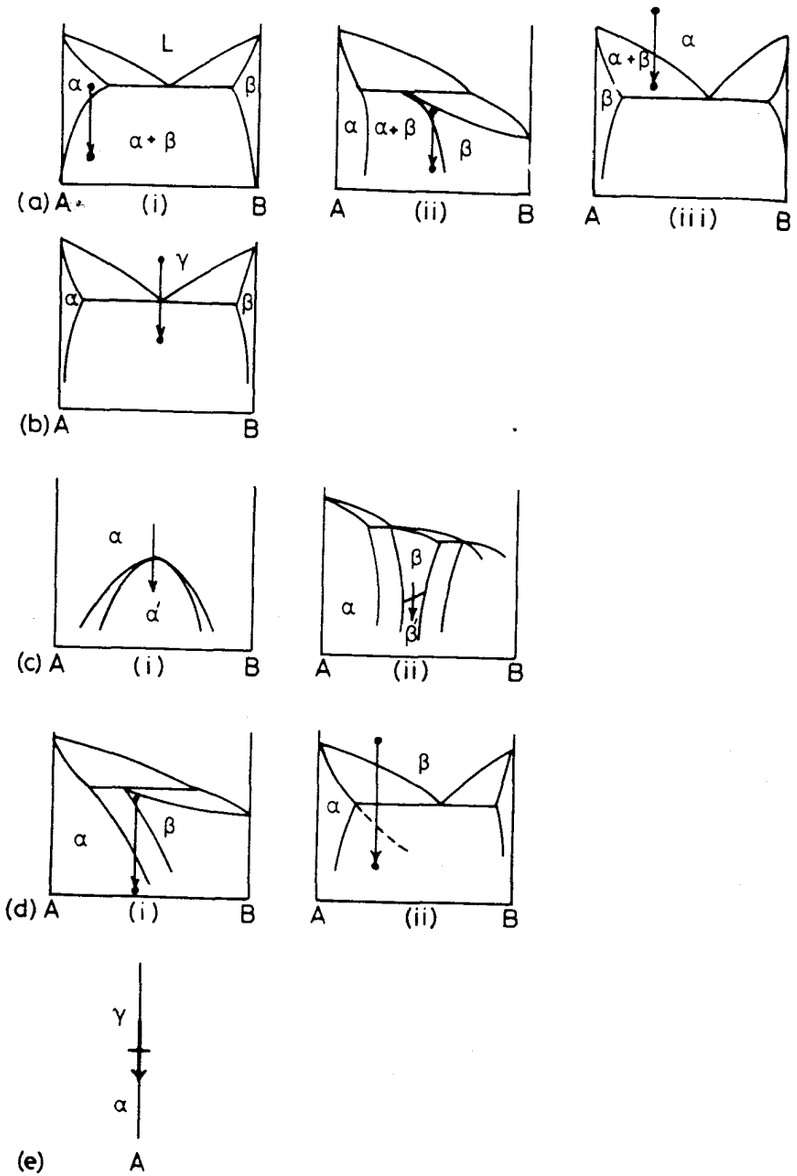

Fig. 5.1 Examples of different categories of diffusional phase transformations: (a) precipitation; (b) eutectoid; (c) ordering; (d) massive; (e) polymorphic (single component).

where only one new phase results. Note that the new β phase can either be stable (Fig. 5.1d(i)) or metastable (Fig. 5.1d(ii)).

Polymorphic transformations occur in single component systems when different crystal structures are stable over different temperature ranges, Fig. 5.1e. The most well-known of these in metallurgy are the transformations between fcc- and bcc-Fe. In practice, however, such transformations are of little practical interest and have not been extensively studied.

Apart from a few exceptions the above transformations all take place by diffusional nucleation and growth. As with solidification, nucleation is usually heterogeneous, but for the sake of simplicity let us begin by considering homogeneous nucleation.

5.1 Homogeneous Nucleation in Solids

To take a specific example consider the precipitation of B-rich β from a supersaturated A-rich α solid solution as shown in Fig. 5.1a(i). For the nucleation of β, B-atoms within the α matrix must first diffuse together to form a small volume with the β composition, and then, if necessary, the atoms must rearrange into the β crystal structure. As with the liquid → solid transformation an α/β interface must be created during the process and this leads to an activation energy barrier.

The free energy change associated with the nucleation process will have the following three contributions.

1. At temperatures where the β phase is stable, the creation of a volume V of β will cause a volume free energy *reduction* of $V\Delta G_v$.
2. Assuming for the moment that the α/β interfacial energy is isotropic the creation of an area A of interface will give a free energy *increase* of $A\gamma$.
3. In general the transformed volume will not fit perfectly into the space originally occupied by the matrix and this gives rise to a misfit strain energy ΔG_s per unit volume of β. (It was shown in Chapter 3 that, for both coherent and incoherent inclusions, ΔG_s is proportional to the volume of the inclusion.) Summing all of these gives the total free energy change as

$$\Delta G = -V\Delta G_v + A\gamma + V\Delta G_s \tag{5.5}$$

Apart from the misfit strain energy term, Equation 5.5 is very similar to that derived for the formation of a solid nucleus in a liquid. With solid/liquid interfaces γ can be treated as roughly the same for all interfaces, but for nucleation in solids γ can vary widely from very low values for coherent interfaces to high values for incoherent interfaces. Therefore the $A\gamma$ term in Equation 5.5 should really be replaced by a summation over all surfaces of the nucleus $\Sigma\gamma_i A_i$.

If we ignore the variation of γ with interface orientation and assume the nucleus is spherical with a radius of curvature r Equation 5.5 becomes

$$\Delta G = -\frac{4}{3}\pi r^3(\Delta G_v - \Delta G_s) + 4\pi r^2\gamma \tag{5.6}$$

This is shown as a function of r in Fig. 5.2. Note that the effect of the misfit strain energy is to reduce the effective driving force for the transformation to $(\Delta G_v - \Delta G_s)$. Similar curves would in fact be obtained for any nucleus shape as a function of its size. Differentiation of Equation 5.6 yields

$$r^* = \frac{2\gamma}{(\Delta G_v - \Delta G_s)} \tag{5.7}$$

$$\Delta G^* = \frac{16\pi\gamma^3}{3(\Delta G_v - \Delta G_s)^2} \tag{5.8}$$

which is very similar to the expressions for solidification, except now the chemical driving force ΔG_v is reduced by a positive strain energy term.

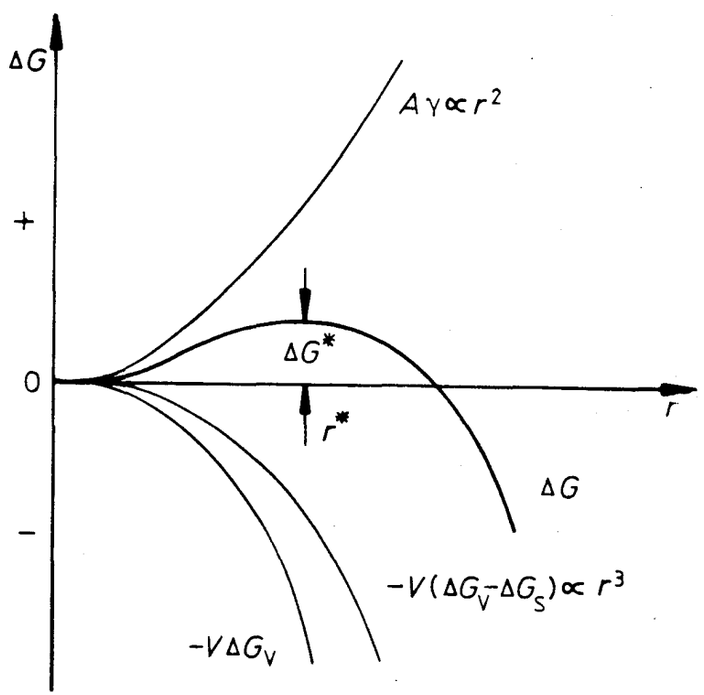

Fig. 5.2 The variation of ΔG with r for a homogeneous nucleus. There is an activation energy barrier ΔG^*.

As discussed in Chapter 4 the concentration of critical-sized nuclei C^* will be given by

$$C^* = C_0 \exp(-\Delta G^*/kT) \tag{5.9}$$

where C_0 is the number of atoms per unit volume in the phase. If each nucleus can be made supercritical at a rate of f per second the homogeneous nucleation rate will be given by

$$N_{hom} = fC^* \tag{5.10}$$

f depends on how frequently a critical nucleus can receive an atom from the α matrix. This will depend on the surface area of the nucleus and the rate at which diffusion can occur. If the activation energy for atomic migration is ΔG_m per atom, f can be written as $\omega \exp(-\Delta G_m/kT)$ where ω is a factor that includes the vibration frequency of the atoms and the area of the critical nucleus. The nucleation rate will therefore be of the form

$$N_{hom} = \omega C_0 \exp\left(-\frac{\Delta G_m}{kT}\right) \exp\left(-\frac{\Delta G^*}{kT}\right) \tag{5.11}$$

This is essentially identical to Equation 4.12 except that the temperature dependence of f has been taken into account. In order to evaluate this equation as a function of temperature ω and ΔG_m can be assumed to be constant, but ΔG^* will be strongly temperature dependent. The main factor controlling ΔG^* is the driving force for precipitation ΔG_v, Equation 5.8. Since composition is variable the magnitude of ΔG_v must be obtained from the free energy–composition diagram.

If the alloy X_0 in Fig. 5.3, is solution treated at T_1 and then cooled rapidly to T_2 it will become supersaturated with B and will try to precipitate β. When the transformation to $\alpha + \beta$ is complete the free energy of the alloy will have decreased by an amount ΔG_0 per mole as shown in Fig. 5.3b. ΔG_0 is therefore the total driving force for the transformation. However, it is not the driving force for *nucleation*. This is because the first nuclei to appear do not significantly change the α composition from X_0. The free energy released per mole of nuclei formed can be obtained as follows.

If a small amount of material with the nucleus composition (X_B^β) is removed from the α phase, the total free energy of the system will *decrease* by ΔG_1 where

$$\Delta G_1 = \mu_A^\alpha X_A^\beta + \mu_B^\alpha X_B^\beta \quad \text{(per mol } \beta \text{ removed)} \tag{5.12}$$

This follows simply from the definition of chemical potential given by Equation 1.29. ΔG_1 is a quantity represented by point P in Fig. 5.3b. If these atoms are now rearranged into the β crystal structure and replaced, the total free energy of the system will *increase* by an amount

$$\Delta G_2 = \mu_A^\beta X_A^\beta + \mu_B^\beta X_B^\beta \quad \text{(per mol } \beta \text{ formed)} \tag{5.13}$$

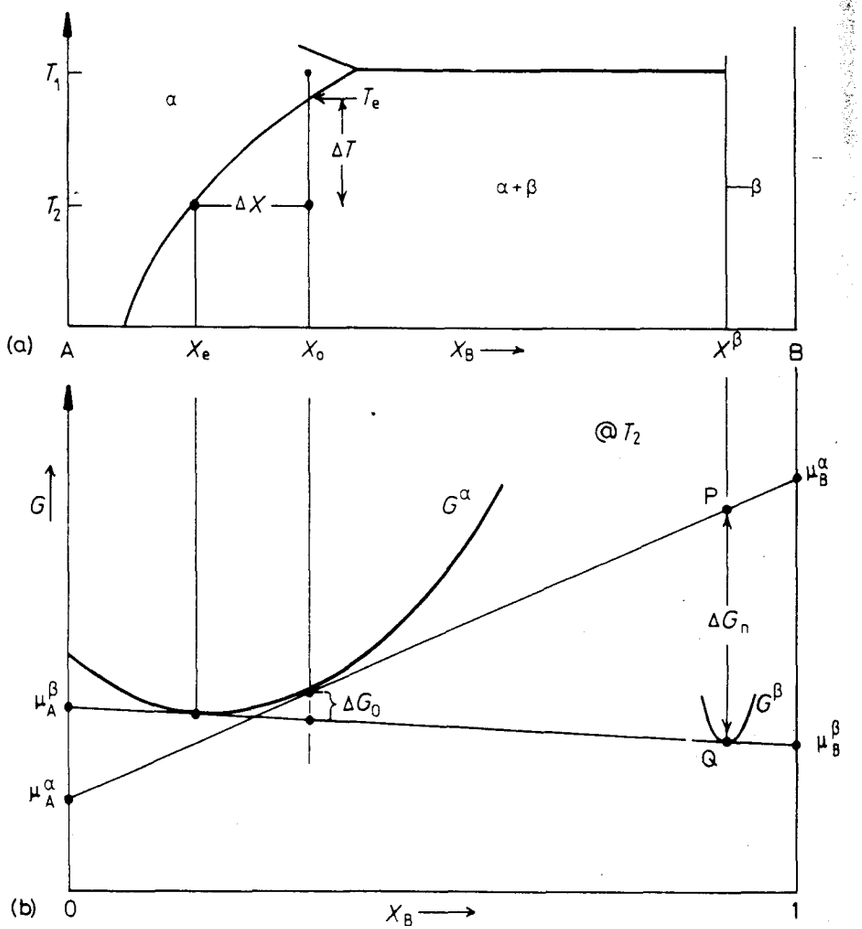

Fig. 5.3 Free energy changes during precipitation. The driving force for the first precipitates to nucleate is $\Delta G_n = \Delta G_v V_m$. ΔG_0 is the total decrease in free energy when precipitation is complete and equilibrium has been reached.

which is given by point Q. Therefore the driving force for nucleation

$$\Delta G_n = \Delta G_2 - \Delta G_1 \quad \text{per mol of } \beta \tag{5.14}$$

which is just the length PQ in Fig. 5.3b. The *volume* free energy decrease associated with the nucleation event is therefore simply given by

$$\Delta G_v = \frac{\Delta G_n}{V_m} \quad \text{per unit volume of } \beta \tag{5.15}$$

where V_m is the molar volume of β. For dilute solutions it can be shown that

approximately

$$\Delta G_v \propto \Delta X \tag{5.16}$$

where

$$\Delta X = X_0 - X_e \tag{5.17}$$

From Fig. 5.3a therefore it can be seen that the driving force for precipitation increases with increasing undercooling (ΔT) below the equilibrium solvus temperature T_e.

It is now possible to evaluate Equation 5.11 for alloy X_0 as a function of temperature. The variation of ΔG_v with temperature is shown schematically in Fig. 5.4b. After taking into account the misfit strain energy term ΔG_s the

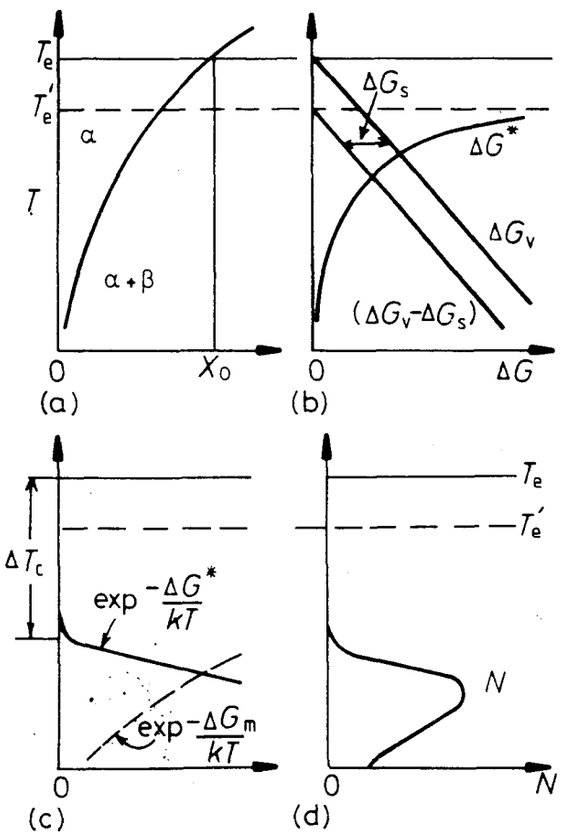

Fig. 5.4 How the rate of homogeneous nucleation varies with undercooling for alloy X_0. (a) The phase diagram. (b) The effective driving force ($\Delta G_v - \Delta G_s$) and the resultant energy barrier ΔG^*. (c) The two exponential terms that determine N as shown in (d).

effective driving force becomes ($\Delta G_v - \Delta G_s$) and the effective equilibrium temperature is reduced to T'_e. Knowing ($\Delta G_v - \Delta G_s$) the activation energy ΔG^* can be calculated from Equation 5.8 as shown. Figure 5.4c shows the two exponential terms in Equation 5.11; $\exp(-\Delta G^*/kT)$ is essentially the potential concentration of nuclei and, as with nucleation in liquids, this is essentially zero until a critical undercooling ΔT_c is reached, after which it rises very rapidly. The other term, $\exp(-\Delta G_m/kT)$, is essentially the atomic mobility. Since ΔG_m is constant this decreases rapidly with decreasing temperature. The combination of these terms, i.e. the homogeneous nucleation rate is shown in Fig. 5.4d. Note that at undercoolings smaller than ΔT_c, N is negligible because the driving force ΔG_v is too small, whereas at very high undercoolings N is negligible because diffusion is too slow. A maximum nucleation rate is obtained at intermediate undercoolings. For alloys containing less solute the critical supercooling will not be reached until lower absolute temperatures where diffusion is slower. The resultant variation of N with T in these alloys will therefore appear as shown in Fig. 5.5.

In the above treatment of nucleation it has been assumed that the nucleation rate is constant. In practice however the nucleation rate will initially be low, then gradually rise, and finally decrease again as the first nuclei to form start growing and thereby reduce the supersaturation of the remaining α.

It has also been assumed that the nuclei are spherical with the equilibrium composition and structure of the β phase. However, in practice nucleation will be dominated by whatever nucleus has the minimum activation energy barrier ΔG^*. Equation 5.8 shows that by far the most effective way of minimizing ΔG^* is by the formation of nuclei with the smallest total interfacial energy. In fact this criterion is dominating in nucleation processes. Incoherent nuclei have such a high value of γ that incoherent homogeneous nucleation is virtually impossible. If, however, the nucleus has an *orientation relationship* with the matrix, and coherent interfaces are formed, ΔG^* is greatly reduced

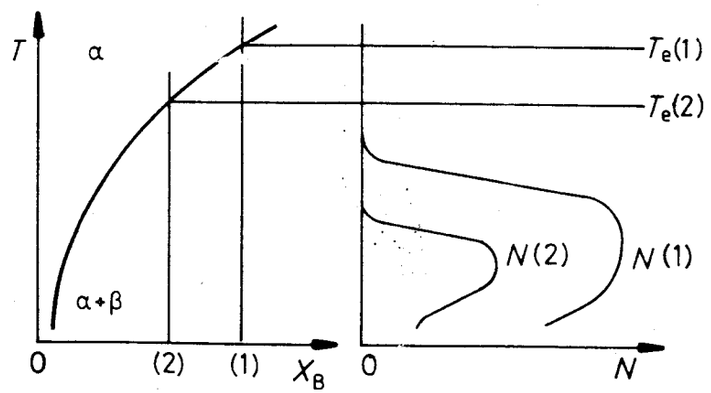

Fig. 5.5 The effect of alloy composition on the nucleation rate. The nucleation rate in alloy 2 is always less than in alloy 1.

and homogeneous nucleation becomes feasible. The formation of a coherent nucleus will of course increase ΔG_s which decreases T'_e. But below T'_e the decrease in γ resulting from coherency can more than compensate for the increase in ΔG_s. Also, by choosing a suitable shape it is often possible to minimize ΔG_s as discussed in Section 3.4.3.

In most systems the α and β phases have such different crystal structures that it is impossible to form coherent low-energy interfaces and homogeneous nucleation of the equilibrium β phase is then impossible. However, it is often possible to form a coherent nucleus of some other, metastable phase (β′) which is not present in the equilibrium phase diagram. The most common example of this is the formation of GP zones which will be discussed in more detail later.

There are a few systems in which the equilibrium phase may nucleate homogeneously. For example in the Cu–Co system Cu alloys containing 1–3% Co can be solution treated and quenched to a temperature where Co precipitates. Both Cu and Co are fcc with only a 2% difference in lattice parameter. Therefore very little coherency strain is associated with the formation of coherent Co particles. The interfacial energy is about 200 mJ m^{-2} and the critical undercooling for measurable homogeneous nucleation is about 40 °C. This system has been used to experimentally test the theories of homogeneous nucleation and reasonably close agreement was found[1].

Another system in which the equilibrium phase is probably formed homogeneously at a few tens of degrees undercooling is the precipitation of Ni_3Al in many Ni-rich alloys. Depending on the system the misfit varies up to a maximum of 2%, and γ is probably less than 30 mJ m^{-2}. Most other examples of homogeneous nucleation, however, are limited to metastable phases, usually GP zones. (See Section 5.5.1.)

5.2 Heterogeneous Nucleation

Nucleation in solids, as in liquids, is almost always heterogeneous. Suitable nucleation sites are non-equilibrium defects such as excess vacancies, dislocations, grain boundaries, stacking faults, inclusions, and free surfaces, all of which increase the free energy of the material. If the creation of a nucleus results in the destruction of a defect, some free energy (ΔG_d) will be released thereby reducing (or even removing) the activation energy barrier. The equivalent to Equation 5.5 for heterogeneous nucleation is

$$\Delta G_{het} = -V(\Delta G_v - \Delta G_s) + A\gamma - \Delta G_d \qquad (5.18)$$

Nucleation on Grain Boundaries

Ignoring any misfit strain energy, the optimum embryo shape should be that which minimizes the total interfacial free energy. The optimum shape for an *incoherent* grain-boundary nucleus will consequently be two abutted spherical

caps as shown in Fig. 5.6, with θ given by

$$\cos\theta = \gamma_{\alpha\alpha}/2\gamma_{\alpha\beta} \tag{5.19}$$

(assuming $\gamma_{\alpha\beta}$ is isotropic and equal for both grains). The excess free energy associated with the embryo will be given by

$$\Delta G = -V\Delta G_v + A_{\alpha\beta}\gamma_{\alpha\beta} - A_{\alpha\alpha}\gamma_{\alpha\alpha} \tag{5.20}$$

where V is the volume of the embryo, $A_{\alpha\beta}$ is the area of α/β interface of energy $\gamma_{\alpha\beta}$ created, and $A_{\alpha\alpha}$ the area of α/α grain boundary of energy $\gamma_{\alpha\alpha}$ destroyed during the process. The last term of the above equation is simply ΔG_d in Equation 5.18.

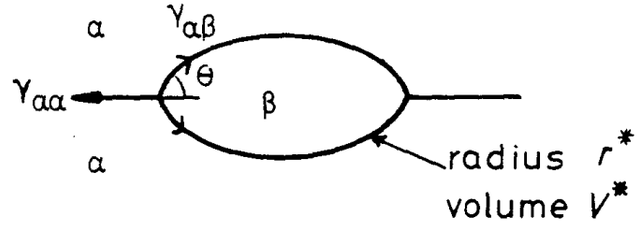

Fig. 5.6 The critical nucleus size (V^*) for grain boundary nucleation.

It can be seen that grain boundary nucleation is analogous to solidification on a substrate (Section 4.1.3) and the same results will apply. Again the critical radius of the spherical caps will be independent of the grain boundary and given by

$$r^* = 2\gamma_{\alpha\beta}/\Delta G_v \tag{5.21}$$

and the activation energy barrier for heterogeneous nucleation will be given by

$$\frac{\Delta G^*_{het}}{\Delta G^*_{hom}} = \frac{V^*_{het}}{V^*_{hom}} = S(\theta) \tag{5.22}$$

where $S(\theta)$ is a shape factor given by

$$S(\theta) = \frac{1}{2}(2 + \cos\theta)(1 - \cos\theta)^2 \tag{5.23}$$

The ability of a grain boundary to reduce ΔG^*_{het}, i.e. its potency as a nucleation site, depends on cos θ, i.e. on the ratio $\gamma_{\alpha\alpha}/2\gamma_{\alpha\beta}$.

V^* and ΔG^* can be reduced even further by nucleation on a grain edge or grain corner, Figs. 5.7 and 5.8. Figure 5.9 shows how $\Delta G^*_{het}/\Delta G^*_{hom}$ depends on cos θ for the various grain boundary nucleation sites.

High-angle grain boundaries are particularly effective nucleation sites for incoherent precipitates with high $\gamma_{\alpha\beta}$. If the matrix and precipitate are sufficiently compatible to allow the formation of lower energy facets then V^* and

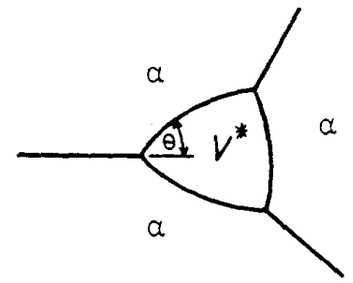

Fig. 5.7 Critical nucleus shape for nucleation on a grain edge.

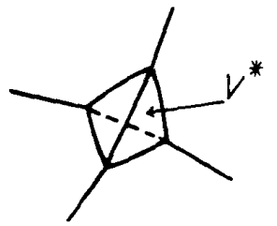

Fig. 5.8 Critical nucleus shape for nucleation on a grain corner.

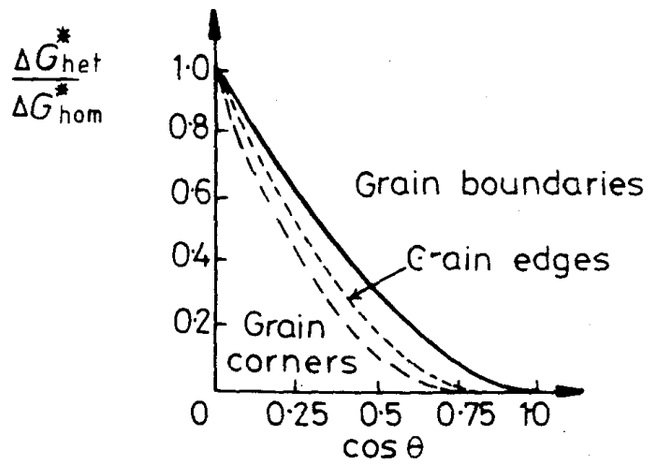

Fig. 5.9 The effect of θ on the activation energy for grain boundary nucleation relative to homogeneous nucleation. (After J.W. Cahn, *Acta Metallurgia* **4** (1956) 449.)

ΔG^*_{het} can be further reduced as shown in Fig. 5.10. The nucleus will then have an orientation relationship with one of the grains. Such nuclei are to be expected whenever possible, since the most successful nuclei, i.e. those which form most rapidly, will have the smallest nucleation barrier.

Other planar defects such as inclusion/matrix interfaces, stacking faults and free surfaces can behave in a similar way to grain boundaries in reducing ΔG^*. Note, however, that stacking faults are much less potent sites due to their lower energy in comparison to high-angle boundaries.